Efficient electrification with Ga_2O_3 - a robust wide bandgap semiconductor

Authors: Dr. Bill Heffernan[2], Professor Martin Allen[1], Dr. Radnya Mukhedkar[2]

Presenters: Professor Martin Allen[1]

Dr. Bill Heffernan[2]

[1] Department of Electrical and Electrical Engineering, University of Canterbury, Christchurch.

[2] Electric Power Engineering Centre (EPECentre), University of Canterbury, Christchurch.

EEA Conference & Exhibition 2021, 30 June – 1 July, Wellington.

Abstract

Wide bandgap devices are the future of power electronics and traditional silicon based technology. Due to the ability of being switched at very high frequency, wide bandgap devices enable high power density and efficient power electronics systems. Today the application is limited to lower voltage and current ratings at relatively high cost, due to limited device performance as a result of limited understanding of the behaviour of defects. Significant research is being undertaken worldwide to overcome the limitations.

This publication reviews work undertaken at University of Canterbury in collaboration with universities in the US and Australia, in the development of beta gallium oxide (β- Ga_2O_3) to replace the underlying material used in power electronics. β- Ga_2O_3 has demonstrated enormous potential, outstanding theoretical figures-of-merit that are 4−10 times higher than silicon and alternative materials, SiC and GaN, under development. Furthermore, robust performance of β- Ga_2O_3 at high temperatures up to 500°C reducing the requirements on ancillary cooling systems, reduces the weight of the overall solution whilst improving system efficiency.

β- Ga_2O_3 devices and the benefits they bring open doors reduced size and weight, high energy density efficient power conversion technologies suitable for operation in harsh an remote environments. They have the capacity to increase transport range through improved mobile energy conversion (batteries, fuel cells etc.), efficient collection and conversion of power from renewable sources such as wave and wind, high temperature drives for applications in harsh environments such as geothermal plants etc.

Introduction of wide bandgap devices into the power and electrification can be accelerated through the development of matrix switches where a number of these devices are connected in series and parallel to provide the high voltage and current rating. This publication will demonstrate the challenges associated with the operation, control and protection of a multi-device array, primary among them being balancing current and voltage; and conceptualise potential solutions.

The need for improved power electronic switching devices

Limiting climate change can be effected by replacing fossil-fuel powered industrial, commercial and residential processes, and means of transport, with renewable electricity powered ones. To achieve this goal, faster, cheaper, lighter, and more-efficient power electronic switching devices will be needed to reduce the energy losses involved in renewable electricity production, delivery, and usage.

Today, most electrical and electronic products, from small personal items such as mobile-phone chargers, through LED light bulbs, heat-pumps, modern refrigerators, distributed solar generation inverters, electric vehicle chargers, irrigation-pump drives, right up to the high voltage DC link, employ power electronic switching devices for power processing and/or conversion. This is because they have enabled efficient conversion of electric power from one voltage to another and from AC to DC and vice-versa, with no moving parts. Dependent on the control system driving the switching devices, such converter products can be made to source power or to consume it, presenting resistive, capacitive or inductive impedance to the AC network, which can change as a function of voltage. Some products can thus provide voltage support, others can behave as pure resistive loads, while still others can perform as constant power loads.

A good vehicle for describing typical power electronic converter circuits is the PV solar inverter, which generally actually comprises two converters and can display many interesting operating modes.

The first converter, which is generally an H-bridge, galvanically isolates the PV solar panels from the mains network, for safety reasons. Since the output of the PV panels is DC, this is a DC-DC converter, with transformer isolation, supplying power to the DC bus. It does this by alternately switching the current from the panels in first one direction, then the other, through the transformer primary winding, at a frequency generally in the kHz range. This high-frequency alternating primary current, which is often an approximate square wave, controlled by pulse-width-modulation (PWM), produces an isolated alternating current in the secondary winding, which is rectified and fed into the DC bus capacitors. Thus the DC-DC converter (Figure 1) controls power flow into the DC bus.

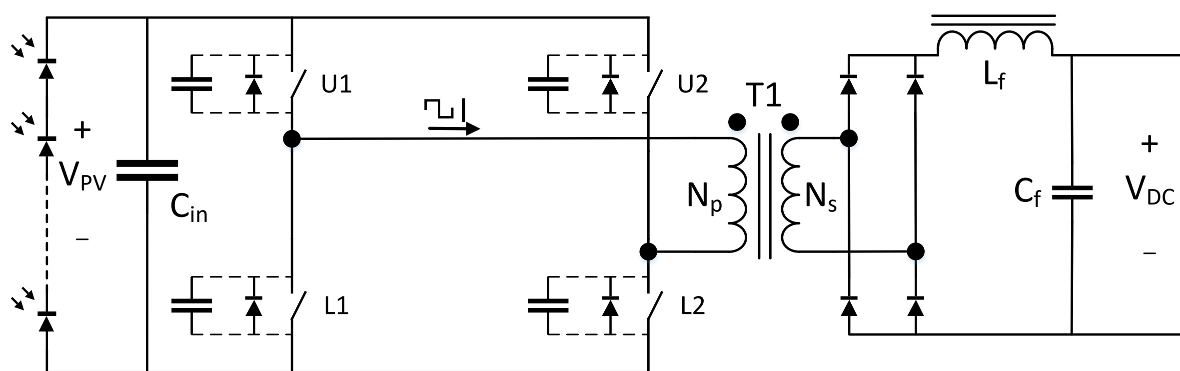

Figure 1. H-Bridge DC-DC converter with HF isolating transformer and LC output filter, powering DC bus from photovoltaic panels.

The second converter is the inverter itself, which generally uses a bridge circuit to alternately switch the DC bus voltage across a circuit consisting of a power control inductor and the local AC mains network (shown for the three-phase case in Figure 2). The switches in this bridge are generally controlled by sinusoidal PWM, in which the DC voltage is chopped into variable

pulse-widths, to give a very good approximation to a sine wave of current through the power control inductor.

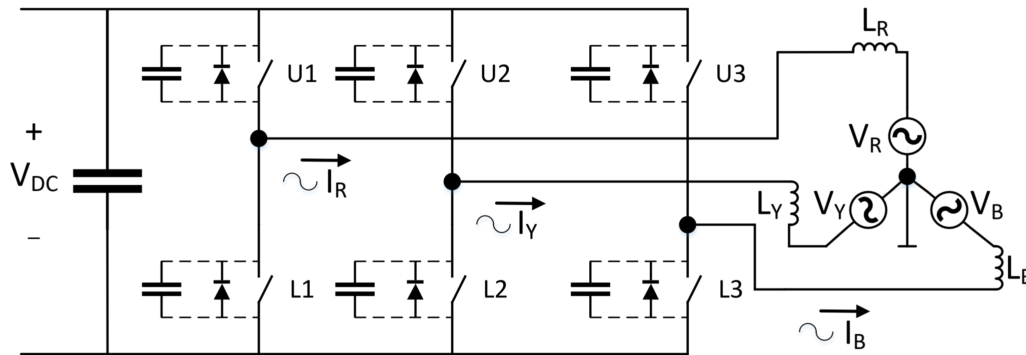

Figure 2. Three-phase inverter, powered from DC bus, showing power control inductors L_R, L_Y and L_B, though which current is injected into, or drawn from the grid at the desired, controllable phase angle.

The two converters must work interactively, as in normal operation the DC-DC converter is trying to operate at the PV array Maximum Power Point (MPP). However, for this to work, there either needs to be some battery storage on the DC bus, or the inverter must be shifting all of this power directly into the AC mains network.

The higher the switching frequency of the DC-DC converter in Figure 1, the smaller, lighter and cheaper can be the isolating transformer, T1, and the DC-side filtering components, L_f and C_f. The higher the switching frequency of the inverter in Figure 2, the smaller, lighter and cheaper the power control inductors, $L_{R,Y,\ B}$ can be and/or the lower the current harmonic distortion into the AC mains network.

Hence, switching devices that can operate faster enable smaller, lighter and cheaper power electronic converters. Since the surface area for cooling a smaller converter with the same power rating is smaller, the switches must also be more efficient, at the increased frequency, or be able to run reliably at higher temperatures, or both.

Beta Gallium Oxide

Beta-phase gallium oxide (β-Ga_2O_3) has recently emerged as an attractive wide bandgap semiconductor with the potential to replace Si, SiC, and GaN in high-efficiency power electronic devices for power electronics control and switching applications [1]–[5]. It has an ultra-wide bandgap (4.85 eV), extremely high breakdown strength (~8 MV/cm), and industry-leading Baliga and Johnson power electronics figures of merit (FOM) that are significantly higher than those of any other existing power electronics material (see Table 1) [1]–[5].

Table I. Comparison of the key material properties of next-generation power electronic materials compared to Si.

	Si	β-Ga_2O_3	SiC	GaN
Bandgap (eV)	1.1	4.8	3.3	3.4
Breakdown Field: E_C (MV/cm)	0.3	8	2.5	3.3
Baliga Figure of Merit:	1	3,444	340	870
Johnson Figure of Merit:	1	2,844	278	1,089

These FOM are defined as $\varepsilon\mu E_C^3$ (Baliga) and $v_{Sat}E_C$ (Johnson) where ε, μ, v_{sat}, and E_C are the dielectric constant, electron mobility, electron saturation velocity, and critical breakdown field, respectively, with the Baliga and Johnson FOMs describing the suitability of a material for high voltage (low loss) and high frequency power electronics devices, respectively.

Like silicon, β-Ga_2O_3 has the outstanding advantage of the availability of large native single crystal wafers produced using inexpensive melt-based bulk-growth methods such as the Czochralski, Floating Zone, Edge-Defined Film-Fed, and Vertical Bridgman techniques, something that is not available for SiC, and GaN, which should lead to significantly lower β-Ga_2O_3 device costs [3], [6], [7]. Its exceptionally high breakdown strength is significantly higher than that of GaN or SiC (~3 MV/cm) and Si (~0.3 MV/cm) and this should allow the key dimensions of power switching diodes and power transistors to be scaled to much smaller sizes, decreasing on-resistance and increasing speed and efficiency [1], [3]. β-Ga_2O_3 is intrinsically insulating with device layers of controllable *n*-type conductivity achieved by doping with Si, Sn, or Ge [1]. The relevant electronic properties of the main power electronics semiconductors are compared in the pentagon diagram of Figure 3 which shows that β-Ga_2O_3 is highly suited for high voltage applications due to its large bandgap and high breakdown strength [4].

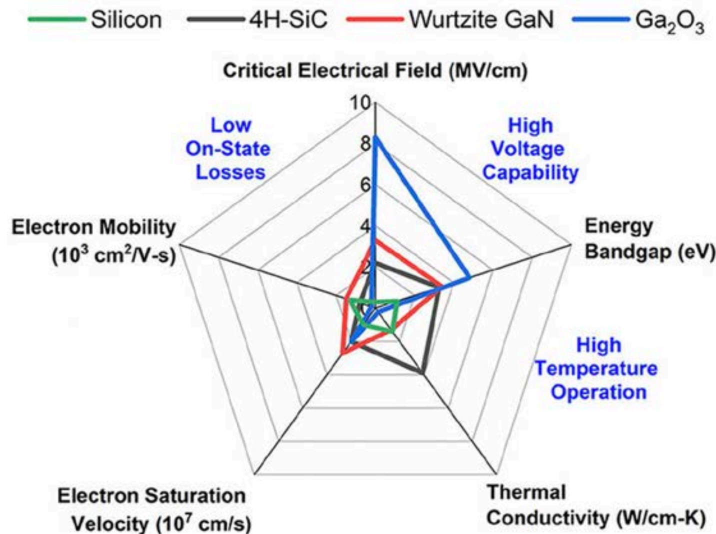

Figure 3. Pentagon diagram shows the important materials properties relevant to power electronics applications. Adapted from Ref. [4].

Figure 4 shows the predicted on-resistance versus breakdown voltage in unipolar power electronic devices (i.e. Schottky diodes and MOSFETs) for β-Ga_2O_3, Si, SiC, and GaN indicating that the conduction losses for β-Ga_2O_3 devices should be approximately 5 to 10 times lower than those for GaN and SiC for the same breakdown voltage, and orders of magnitude better than Si [3].

Another advantage of β-Ga_2O_3 is the reproducible fabrication of high-performance metal-semiconductor Schottky contacts, the key device component in high-speed rectifying Schottky diodes and metal-semiconductor field effect transistors. The key Schottky contact figures-of-merit are its barrier height, which denotes the strength of the rectifying effect (i.e. on- versus off-current), and its ideality factor, which measures the laterally homogeneity of the Schottky contact and which should be close to unity for an ideal contact.

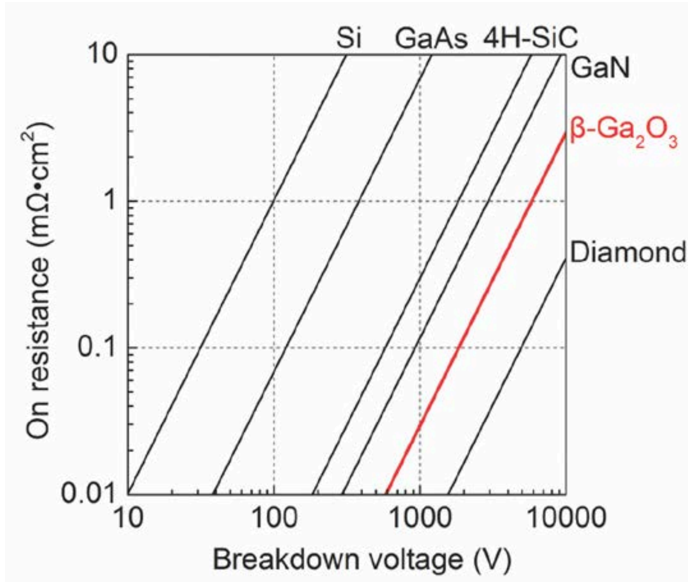

Figure 4. Theoretical on-resistance versus breakdown voltage in unipolar power electronic devices (i.e. Schottky diodes and MOSFETs) for β-Ga_2O_3 compared to other power electronics semiconductors. Adapted from Ref. [3].

Figure 5(a) shows the barrier heights for β-Ga_2O_3 Schottky contacts fabricated using a range of conventional high work-function metals: Pt; Pd; Ir; Ru; Au; and Ag [8], [9]. To dramatically improve device performance, we have recently developed a technology involving the deliberate *in-situ* plasma oxidation of the plain-metal Schottky contact layer during device fabrication that increases the Schottky barrier height by approximately 40–50 % to more than 2.0 eV [8], [9]. This effect is shown in Figure 5(b) with the resulting Schottky barrier height values among the highest-reported for any electronic material. This has the advantage of producing an extremely-strong on/off current rectification effect of more than 9 orders of magnitude with typical off-currents of less than one nanoamp per square centimetre (< 10^{-9} Acm^{-2}) [8], [9].

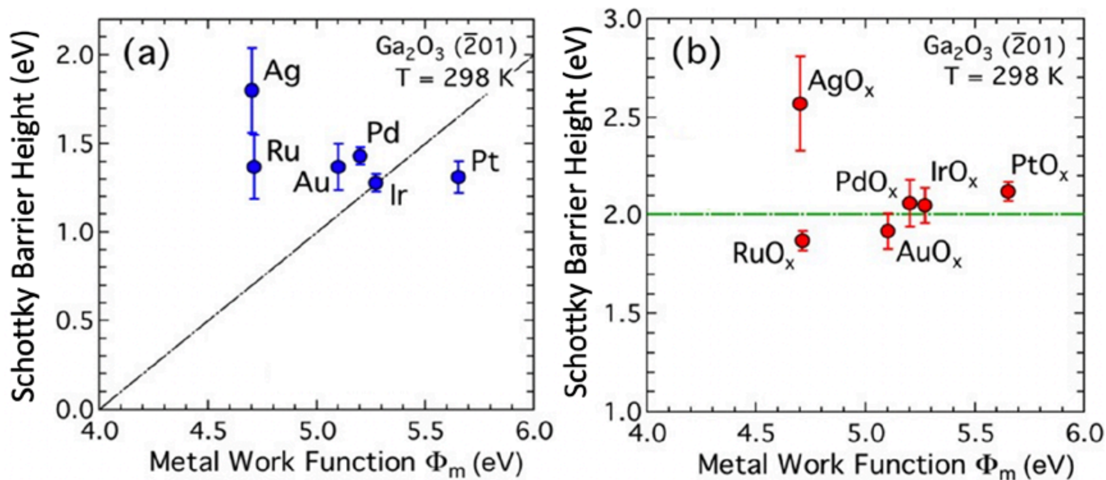

Figure 5. Typical Schottky barrier heights for (a) plain-metal and (b) deliberately-oxidized metal Schottky diodes on β-Ga_2O_3.

In addition, these oxidized-metal β-Ga_2O_3 Schottky contacts, particularly those involving PtO_x, IrO_x, and PdO_x have a very high thermal stability, remaining highly-rectifying up to

temperatures of at least 500 °C with no degradation in ideality factor or contact quality [10]–[13]. The use of these thermally-stable Schottky contacts will allow β-Ga_2O_3 Schottky diodes and metal-semiconductor field effect transistors to operate at much higher temperatures than Si, reducing the size of cooling systems for power electronics whilst mitigating the comparatively low thermal conductivity of β-Ga_2O_3. Figure 6 shows the typical very high temperature performance of oxidized iridium (IrO_x) β-Ga_2O_3 Schottky diodes with very similar results obtained for PtO_x and PdO_x Schottky contact layers. This shows almost no increase in reverse leakage current from room temperature to 350 °C, with rectification ratios (at ± 3 V) of more than 10 orders of magnitude and a steady decrease in on-voltage with temperature. These Schottky diodes were still highly-rectifying while operating at 500 °C, with rectification ratios (at ± 3 V) of 6 orders of magnitude despite many temperature cycles over this range.

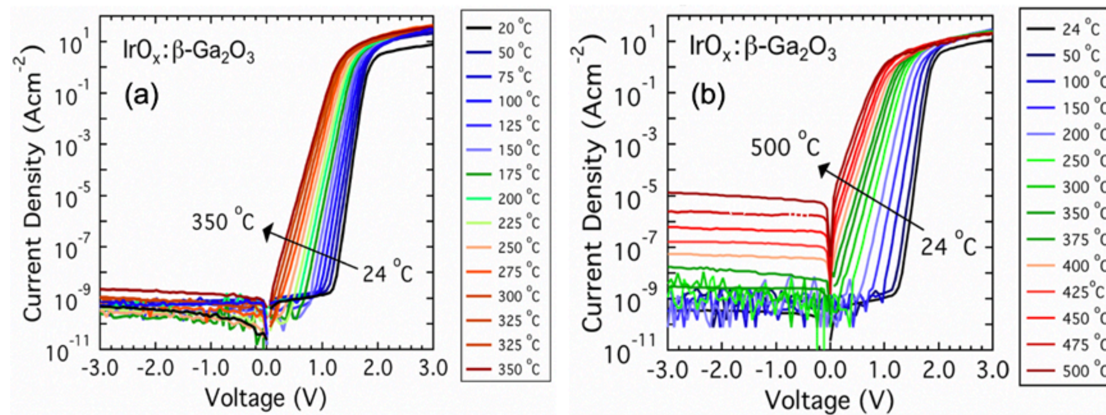

Figure 6. High temperature performance of oxidized Iridium (IrO_x) Schottky diodes on β-Ga_2O_3 from (a) room temperature to 350 °C, and (b) room temperature to 500 °C.

Active switches

The above discussion shows that Ga_2O_3 could, in the relatively near future, offer many of the necessary improvements. At this stage, its use for making Schottky rectifier diodes, which would be ideal as the secondary-side rectifiers in Figure 1, could be its entrée as a serious contender. However, it is worth remembering that advances in semiconductor materials and the development of devices that can be implemented using them, tend to take several years, if not decades, to come to fruition.

Today's large power electronic converters, between about 1MW and 10MW, generally employ Si IGBTs as active switches. This is because IGBTs have low conduction losses (rather like thyristors) as their conduction loss is dominated by the collector-emitter saturation voltage. However, this advantage comes at the cost of relatively low speed switching capability - they are very slow to turn off, because they are bipolar devices and during turn-off the hole and electron charge carriers have to recombine to rebuild the non-conducting depletion region of the off-state device. In practice, this limits switching frequency to a few kHz.

However, IGBTs, which first became available in the 1970s, represent a major improvement over power bipolar junction transistors (BJTs), as they are electric field controlled and hence do not suffer from the very low current gain of large BJTs. Early IGBTs were able to block only around 1kV when off, but over about 30 years they have developed to about 6.5kV. They have therefore, over three decades, been able to displace thyristors in all but very high power applications.

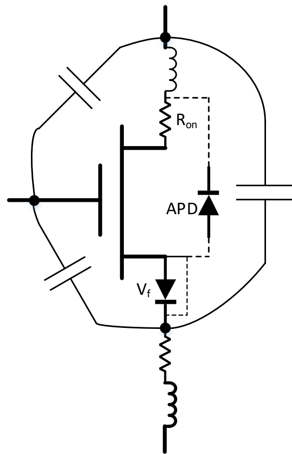

Figure 7. Generic model of a 3-terminal electric field controlled active switching device.

Figure 7 shows a generic model of an active switch device controlled by electric field. It can describe most of the presently-available enhancement-mode (i.e. normally off) power electronic switches, including IGBTs, MOSFETs, Superjunction MOSFETs and HEMTs.

The features of Figure 7 can be used to explain the cause and significance of conduction ("on") losses and switching losses in a device. Conduction losses are almost independent of switching frequency, while switching losses are proportional to it.

Conduction losses

With IGBTs, the conduction losses are dominated by collector-emitter saturation voltage (modelled here by diode forward drop voltage, V_f), of about 2V. The resistive component of the conduction path when an IGBT is on, R_{on}, is generally negligible, such that the conduction losses are given by I x V_f, where I is the average current through the IGBT. With MOSFETs and HEMTs being unipolar devices, there is no saturation voltage, so V_f is shorted out and R_{on} dominates the conduction losses, such that they are given by I^2 x R_{on}, where I is the RMS current through the MOSFET/HEMT. Semiconductors with lower specific on-resistance, for a given voltage breakdown rating, are at a considerable advantage here.

Switching losses

Losses occur both at turn-on and at turn-off. For all these electric field controlled devices, charge must be injected into the gate at turn-on. This charges the two capacitors on the left of the device: gate-source capacitance below and gate-drain capacitance above. The gate-source (or gate-emitter) capacitance only has to charge up by a few volts, say from 0 to 10V in a typical MOSFET. On the other hand, the gate-drain capacitance (also called Miller capacitance) has to change voltage from –xV to 0V, where x is the voltage from drain to gate while the switch was off. The total charge necessary to turn on an IGBT or MOSFET is usually given (under test conditions) in the device data sheet. Providing this gate charge causes losses in the gate-drivers which drive them. As the switch turns on, the output capacitance, C_{ds} (or C_{ce}) discharges through the switch, dissipating its energy as heat in the switch itself. In addition to all this there is a linear region, which starts when the gate-source (or gate-emitter) voltage reaches the gate threshold level and continues until all the Miller charge has been supplied. During this time the "switch" has both voltage across it and current through it, so the instantaneous power dissipation is very high.

At turn-off, gate charge needs to be removed to get rid of the electric field between gate and source (or emitter). Again, this requires the gate-source (or gate-emitter) voltage to drop from

about 10V to 0V and the drain (or collector) voltage to increase from close to zero to xV. This again represents further losses in the gate-drivers. As with turn-on, there is a linear region starting when the gate has been pulled down to the threshold voltage pending the removal of all the Miller charge. Again, instantaneous power dissipation is very high. With the IGBT, this is further exacerbated by the turn-off continuing after Miller charge removal, until the depletion region has re-established itself after hole-electron recombination.

Essentially, all the foregoing means that IGBTs will never match the speed of MOSFETs and HEMTs, and that MOSFETs or HEMTs that have the lowest specific on-resistance can have the smallest active area, which is likely to translate into the smallest capacitances and hence the lowest overall losses.

But, commercial Ga_2O_3 active devices are not yet available. The next best bet, according to Figure 4, is GaN. Fortunately, a range of GaN HEMTs are now available from half a dozen manufacturers. Unfortunately, the largest readily available device at present is rated at 650V, 60A, with an on-resistance of about 25mΩ [14]. Assuming an application for a 1000V, 1000A switch for a 1MW solar PV DC-DC converter, as in Figure 1, what options could we consider?

Matrix switch concept

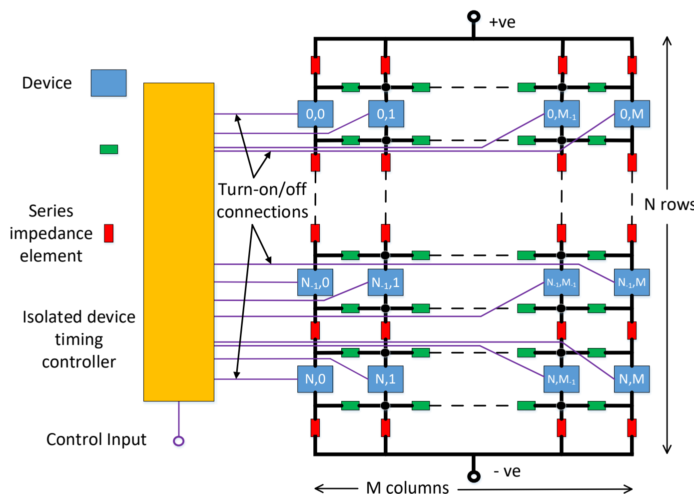

Figure 8. Matrix switch consisting of N rows and M columns of individual devices.

By arranging a number of relatively small devices in a matrix, with N rows to share the required blocking voltage and M columns to share the required conduction current, a composite switch can be built (Figure 8). To avoid damaging individual devices it is essential that the voltage is shared evenly during the off-state and during turn-on and turn-off transients. Similarly, it is necessary to ensure that the current is evenly shared between columns. If the device conduction losses are dominated by on-resistance with a positive temperature co-efficient, there will be a natural tendency to share current in steady-state, but mismatches in the series inductance of individual columns will affect sharing during turn-on and turn-off transients.

Devices are somewhat tolerant to short pulses of high current, the allowable magnitude of which is generally limited by thermal impedance and temperature rise, but intolerant to any overvoltage (although they may be able to absorb a certain amount of avalanche energy before breakdown). Therefore, the voltage sharing criterion is the most severe. Figure 9 shows a pair of 4-row matrix switches forming one leg of Figure 1. For clarity, only the first column of each switch is shown. Upper and lower switch controllers provide gate control pulses to 4 isolated gate drivers for each column of devices. These are commercially available galvanically isolated

drivers [15] with isolated output power rails, referred to 8 floating reference levels from $L3_{ref}$ to $U0_{ref}$. Figure 10 shows the voltage levels, relative to DC link negative, of these 8 references (equal to device source/emitter voltage), during a full switching cycle, when the ground reference of both upper and lower drivers is equal to half DC bus voltage.

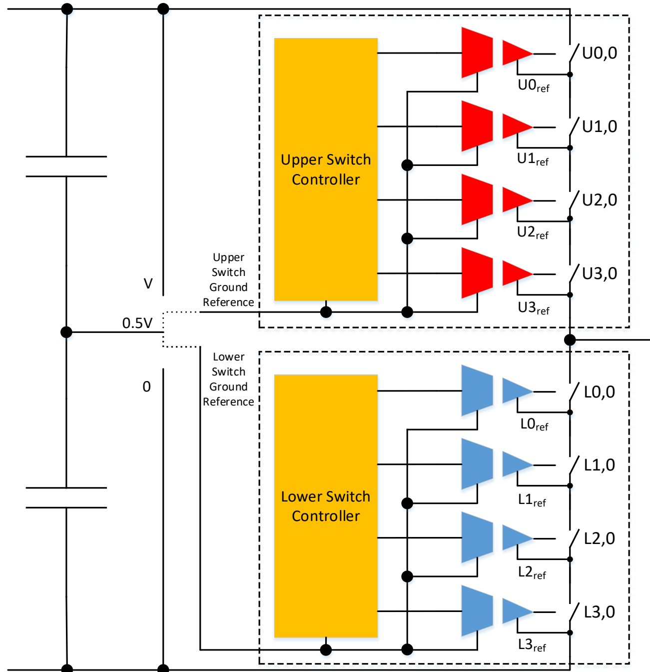

Figure 9. Matrix switches forming one leg of an H-bridge.

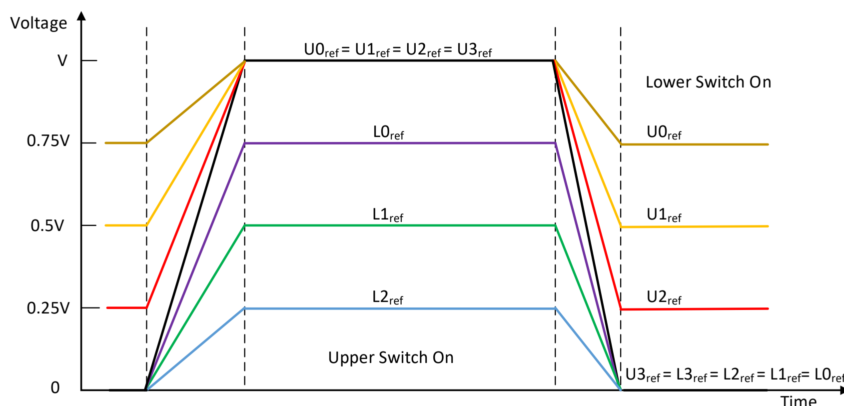

Figure 10. Values of isolated driver reference voltages, with respect to DC link negative.

In Figure 10, all devices are shown turning on and off at exactly the same time and speed; i.e. the dv/dt across each device in the column is precisely the same. In practice, this will not be the case, for several reasons: firstly, both the isolated device drivers and the devices themselves will have slightly different signal propagation and turn-on/turn-off delay times; secondly, they will have slightly different rise and fall times; and thirdly, the device output capacitances will not be identical. Therefore, the traces in Figure 10 will be somewhat offset along the x-axis and will have slightly differing slopes during the transitions. By monitoring the dv/dt of each of the devices in the leg, the switch controllers can alter the precise instants of applying the gate control pulses to minimize the maximum transient voltage experienced by any single device.

Assuming we can build such a switch, rated at 1000V, 1000A, using the 650V, 60A, 25mΩ GaN HEMT devices [14] we can then compare its theoretical performance with that of a typical silicon IGBT module [16] in the 1MW solar PV DC-DC converter of Figure 1.

To normalize the conduction losses, consider that the converter is operating at full power with a duty-cycle of 50%, with a square-wave current of 1000A in each switch and a DC bus voltage of 1000V. The IGBT module has a V_{cesat} of 2V. Therefore, the matrix switch must have an on-resistance of 2mΩ to give V_{ds} of 2V at 1000A. To withstand 1000V, two rows of devices are needed, giving 50mΩ per column. Thus, 25 columns are required. Using data sheet values for gate charge, turn-off plus turn-on energy loss per cycle, turn-on time (encompassing turn-on delay and rise time) and turn-off time (encompassing turn-of delay and fall time), switching losses as a function of frequency can be calculated. Table II compares these values for the single IGBT module, a single GaN HEMT and the matrix of 2 x 25 GaN HEMTs.

Table II. Comparison of switching parameters of Si IGBT module and GaN Matrix Switch.

Parameter	Si IGBT x 1	GaN HEMT x 1	GaN HEMT x 50
Q_g, nC	9,250	14.2	710
E_{cycle}, mJ	260	0.1681	8.405
t_{on}, ns	610	17	17
t_{off}, ns	930	36.9	36.9

Clearly the theoretical GaN matrix switch is very much faster, has far lower switching energy losses and a much lower gate charge requirement. Figure 11 shows the switching losses as a function of frequency for a single instance of the two switch options, in the 1MW converter of Figure 1.

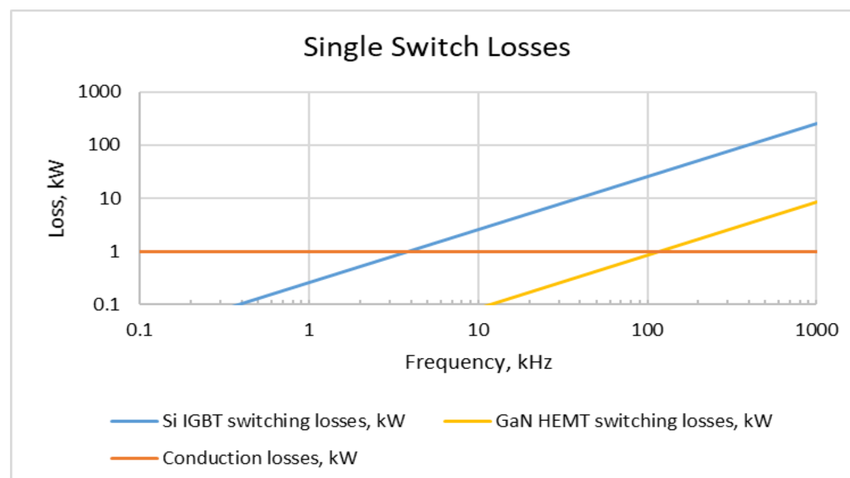

Figure 11. Comparison of losses in Si IGBT module and GaN Matrix Switch

Since both switches are designed to carry 1000A continuously, at which point they would each be dissipating 2kW, it is thermally possible to run them in this 50% duty-cycle application, up to the frequency at which the total loss per switch is 2kW. Given that the conduction losses of each switch option are the same, at 1kW, the maximum frequency occurs when the switching loss lines cross the conduction loss line. For the IGBT option this is at 3.85kHz, while for the HEMT matrix it is at 119kHz. Therefore the converter of Figure 1 can theoretically run at 30 times the frequency with the matrix switch option, greatly reducing the size of the isolation transformer, filter inductor and filter capacitors. Similarly, in the circuit of Figure 2, the increased switching frequency capability can greatly reduce the size of the power-flow control inductors and/or the level of current harmonic distortion injected into the grid.

Conclusions

New semiconductor materials and switching devices will revolutionize grid-connected power electronics in the coming decades. But, new semiconductors and devices made with them can take many years, or even decades, to achieve their full potential. By incorporating emerging devices in matrix switches, their advantages can be realized much sooner.

References

[1] H. Masataka *et al.*, "Recent progress in Ga2O3 power devices," *Semicond. Sci. Technol.*, vol. 31, no. 3, p. 34001, 2016, [Online]. Available: http://stacks.iop.org/0268-1242/31/i=3/a=034001.

[2] H. Zhang *et al.*, "Progress of Ultra-Wide Bandgap Ga2O3 Semiconductor Materials in Power MOSFETs," *IEEE Trans. Power Electron.*, vol. 35, no. 5, pp. 5157–5179, 2020, doi: 10.1109/TPEL.2019.2946367.

[3] M. Baldini, Z. Galazka, and G. Wagner, "Recent progress in the growth of β-Ga2O3 for power electronics applications," *Mater. Sci. Semicond. Process.*, vol. 78, pp. 132–146, 2018, doi: 10.1016/j.mssp.2017.10.040.

[4] S. J. Pearton, F. Ren, M. Tadjer, and J. Kim, "Perspective: Ga2O3 for ultra-high power rectifiers and MOSFETS," *J. Appl. Phys.*, vol. 124, p. 220901, 2018, doi: 10.1063/1.5062841.

[5] S. J. Pearton *et al.*, "A review of Ga2O3 materials, processing, and devices," *Appl. Phys. Rev.*, vol. 5, no. 1, p. 011301, 2018, doi: 10.1063/1.4977857.

[6] H. F. Mohamed, C. Xia, Q. Sai, H. Cui, M. Pan, and H. Qi, "Growth and fundamentals of bulk β-Ga2O3 single crystals," *J. Semicond.*, vol. 40, p. 011801, 2019, doi: 10.1088/1674-4926/40/1/011801.

[7] A. Kuramata, K. Koshi, S. Watanabe, Y. Yamaoka, T. Masui, and S. Yamakoshi, "High-quality β-Ga2O3 single crystals grown by edge-defined film-fed growth," *Jpn. J. Appl. Phys*, vol. 55, p. 1202A2, 2016, doi: 10.7567/JJAP.55.1202A2.

[8] C. Hou, R. M. Gazoni, R. J. Reeves, and M. W. Allen, "Direct comparison of plain and oxidized metal Schottky contacts on β-Ga2O3," *Appl. Phys. Lett.*, vol. 114, no. 3, p. 033502, 2019, doi: 10.1063/1.5079423.

[9] C. Hou, R. M. Gazoni, R. J. Reeves, and M. W. Allen, "Oxidized Metal Schottky Contacts on (010) β-Ga2O3," *IEEE Electron Device Lett.*, vol. 40, no. 2, pp. 337–340, 2019, doi: 10.1109/LED.2019.2891304.

[10] C. Hou *et al.*, "High-temperature (350 °C) oxidized iridium Schottky contacts on β-Ga2O3," *Appl. Phys. Lett.*, vol. 114, p. 233503, 2019, doi: 10.1063/1.5099126.

[11] C. Hou, R. M. Gazoni, R. J. Reeves, and M. W. Allen, "High-Temperature β-Ga2O3 Schottky Diodes and UVC Photodetectors using RuOx Contacts," *IEEE Electron Device Lett.*, vol. 40, no. 10, pp. 1587–1590, 2019, doi: 10.1109/led.2019.2937494.

[12] C. Hou *et al.*, "High temperature (500 °C) operating limits of oxidized platinum group metal (PtOx, IrOx, PdOx, RuOx) Schottky contacts on β-Ga2O3," *Appl. Phys. Lett.*, vol. 117, p. 203502, 2020, doi: 10.1063/5.0026345.

[13] C. Hou, R. M. Gazoni, R. J. Reeves, and M. W. Allen, "Dramatic Improvement in the Rectifying Properties of Pd Schottky Contacts on β-Ga2O3 During Their High-Temperature Operation," *IEEE Trans. Electron Devices*, vol. 68, no. 4, pp. 1791–1797, 2021, doi: 10.1109/TED.2021.3060689.

[14] GaN Systems GS66516T, 650V E-mode GaN transistor Preliminary Data Sheet, 2018.

[15] Infineon 1EDF5663H, Isolated gate-drive IC for e-mode GaN HEMTs Data Sheet, Rev. 2.3, 2020.

[16] Infineon FZ1200R12HE4 IGBT-Module Data Sheet, 2015.